

## Ultrasensitive Atomic Comagnetometer with Enhanced Nuclear Spin Coherence

Kai Wei,<sup>1,2</sup> Tian Zhao,<sup>1,2</sup> Xiujie Fang,<sup>2,3</sup> Zitong Xu,<sup>1,2</sup> Chang Liu,<sup>1,2</sup> Qian Cao,<sup>1,2</sup> Arne Wickenbrock<sup>4,5</sup>, Yanhui Hu<sup>6,\*</sup>, Wei Ji<sup>4,5,†</sup>, Jiancheng Fang,<sup>1,2</sup> and Dmitry Budker<sup>4,5,7</sup>

<sup>1</sup>*School of Instrumentation Science and Opto-electronics Engineering, Beihang University, Beijing, 100191, China*

<sup>2</sup>*Hangzhou Extremely Weak Magnetic Field Major Science and Technology Infrastructure Research Institute, Hangzhou, 310051, China*


<sup>3</sup>*School of Physics, Beihang University, Beijing 100191, China*

<sup>4</sup>*Helmholtz-Institut, GSI Helmholtzzentrum für Schwerionenforschung, Mainz 55128, Germany*

<sup>5</sup>*Johannes Gutenberg University, Mainz 55128, Germany*

<sup>6</sup>*Department of Physics, King's College London, Strand, London WC2R 2LS, United Kingdom*

<sup>7</sup>*Department of Physics, University of California, Berkeley, California 94720-7300, USA*

 (Received 22 October 2022; accepted 9 January 2023; published 10 February 2023)

Achieving high energy resolution in spin systems is important for fundamental physics research and precision measurements, with alkali-noble-gas comagnetometers being among the best available sensors. We found a new relaxation mechanism in such devices, the gradient of the Fermi-contact-interaction field that dominates the relaxation of hyperpolarized nuclear spins. We report on precise control over spin distribution, demonstrating a tenfold increase of nuclear spin hyperpolarization and transverse coherence time with optimal hybrid optical pumping. Operating in the self-compensation regime, our <sup>21</sup>Ne-Rb-K comagnetometer achieves an ultrahigh inertial rotation sensitivity of  $3 \times 10^{-8}$  rad/s/Hz<sup>1/2</sup> in the frequency range from 0.2 to 1.0 Hz, which is equivalent to the energy resolution of  $3.1 \times 10^{-23}$  eV/Hz<sup>1/2</sup>. We propose to use this comagnetometer to search for exotic spin-dependent interactions involving proton and neutron spins. The projected sensitivity surpasses the previous experimental and astrophysical limits by more than 4 orders of magnitude.

DOI: [10.1103/PhysRevLett.130.063201](https://doi.org/10.1103/PhysRevLett.130.063201)

Coherent control of electron and nuclear spins via light-matter interactions is an important platform for fundamental physics research [1] and an essential tool for quantum sensors [2–4] and quantum information processing [5,6]. A dense mixture of vapors of polarized alkali-metal atoms and noble gases with hyperpolarized nuclei have found prominent use in quantum-technology devices such as atomic magnetometers and comagnetometers, which are used to search for “new physics,” including fifth forces [7,8], axionlike particles [9,10], permanent electric dipole moments [11,12], and to test the combined charge-parity-time (*CPT*) and Lorentz symmetries [13,14].

These applications have long been limited by systematic errors due to magnetic fields from ambient environments or interactions between atoms [15,16]. A typical approach for addressing this problem is to isolate the magnetic-field effect by using two species with different gyromagnetic ratios, for example, <sup>129</sup>Xe and <sup>131</sup>Xe [9,17], <sup>3</sup>He and <sup>129</sup>Xe [11,12], <sup>85</sup>Rb and <sup>87</sup>Rb [18], different nuclear spins in the same molecule [16] or different hyperfine levels of single-species atoms [19]. Another approach is operating the alkali-noble-gas atomic comagnetometer in the self-compensation (SC) regime [4,20], where noble gas nuclear spins interact with alkali electron spins by spin-exchange (SE) interactions and adiabatically cancel slowly changing magnetic fields. Another advantage of the SC comagnetometer is that the

alkali atoms are in the spin-exchange relaxation-free (SERF) regime, achieving sub-femtotesla magnetic sensitivity [21].

The SC mechanism for different alkali-noble-gas pairs varies significantly and is not fully explored. The highest sensitivity in fundamental physics measurements was achieved with long-coherence-time nuclear spin  $I = 1/2$  <sup>3</sup>He-alkali pair [22,23]. However, measurements of exotic interactions may require nuclei with smaller gyromagnetic ratio and/or higher spin, for example, the spin-3/2 <sup>21</sup>Ne [4,14]. Because of the stronger Fermi contact interaction (FCI) between <sup>21</sup>Ne atoms and alkali atoms [24,25], the SC regime is complicated by the strong FCI field from alkali atoms and the quadrupole relaxation as compared to “simpler” <sup>3</sup>He atoms. The SC regime for the heaviest stable-noble-gas <sup>129</sup>Xe, promising for electric dipole moment measurements [26] and quick-start gyroscopes, is also significantly influenced by the larger FCI factor  $\kappa_0$  (two orders of magnitude larger than that for <sup>3</sup>He) and shorter coherence time. In addition, magnetic noise and other main noises in alkali-noble-gas comagnetometer decrease at higher frequencies. Thus the study of breakdown of the SC regime at higher frequency and the development of high-frequency magnetic-noise suppression regime would open new possibility for ultrasensitive comagnetometers.

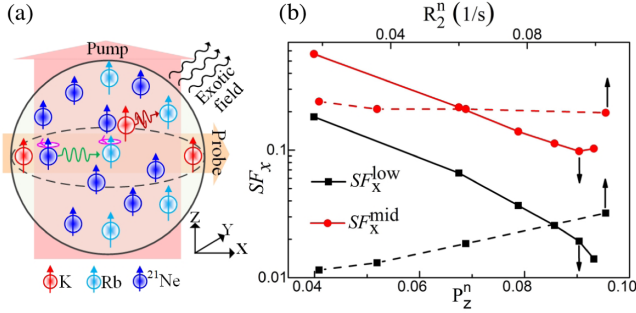


FIG. 1. (a) The pump and probe configuration of the  $^{21}\text{Ne}$ -Rb-K comagnetometer. Hybrid Rb-K atoms are applied to transfer the spin momentum of pumping-light photons to  $^{21}\text{Ne}$  nuclear spins. The precession of  $^{21}\text{Ne}$  spins due to exotic fields or inertial rotation is transferred to the alkali spins, which are read out by probe light based on optical rotation. (b) Suppression factor  $SF_x$  as a function of the noble-gas nuclear spin polarization  $P_z^n$  (solid curves with lower axis) and the noble-gas-spin transverse relaxation rate  $R_2^n$  (dashed curves with upper axis). The  $SF_x^{\text{low}}$  and  $SF_x^{\text{mid}}$  decrease with  $P_z^n$ , and the  $SF_x^{\text{low}}$  increases with  $R_2^n$ , consistent with the theoretical model.

In this Letter, we demonstrate an ultrahigh sensitivity of  $3 \times 10^{-8}$  rad/s/Hz $^{1/2}$  to nonmagnetic perturbations in the low-frequency range in an SC  $^{21}\text{Ne}$ -Rb-K comagnetometer. This is achieved by overcoming the relaxation mechanism of noble-gas nuclear spins related to the gradients of the alkali polarization that is here found to be dominant and that significantly shortens the coherence time and deteriorates the SC performance in various alkali-noble-gas comagnetometers with strong FCI interactions. The influence of hybrid alkali atoms (Rb-K) on spin-polarization homogeneity, hyperpolarization efficiency, and relaxation of noble-gas nuclear spins was theoretically modeled and experimentally optimized, yielding a tenfold increase of coherence time of nuclear spins and the SC suppression ability of the hybrid comagnetometer. The energy sensitivity of this device for exotic field coupling to nuclear spins is on the order of  $10^{-23}$  eV/Hz $^{1/2}$ , which is 6 orders of magnitude better than state-of-art comagnetometers based on Rb atoms [16,19]. This will significantly boost the experiments to search for exotic spin-dependent forces coupled to proton and neutron spins.

A hybrid SC comagnetometer consists of a gaseous mixture of alkali-metal atoms and noble-gas atoms occupying the same glass cell as illustrated in Fig. 1(a). Using hybrid spin-exchange optical pumping (HSEOP), the lower-density alkali species is optically pumped and is used to polarize the higher-density alkali species via SE collisions [27,28]. Simultaneously, electron-spin polarization of the alkali atoms is transferred to noble-gas nuclear spins through SE collisions between them [27]. Under a small external magnetic field, alkali atoms work in the SERF regime. The spin ensembles are pumped along  $\hat{z}$  and are probed along  $\hat{x}$ .

The SE interaction between alkali electron spins and noble-gas nuclear spins couples them together, which can be described by the FCI field seen by one spin species due to the magnetization of the other [20,29]:

$$\tilde{\mathbf{B}}^{n/e} = \frac{2}{3} \kappa_0^{e-n} M_0^{n/e} \mathbf{P}^{n/e}, \quad (1)$$

where the superscripts “e” and “n” denote electron and nuclear spins, respectively;  $\kappa_0^{e-n}$  is the FCI enhancement factor [24];  $\mathbf{P}^e = \langle \mathbf{S}_e \rangle / S_e$  is the collective polarization of alkali electron spins,  $\mathbf{P}^n = \langle \mathbf{K}_n \rangle / K_n$  for noble-gas nuclear spins;  $M_0^e$  and  $M_0^n$  are the magnetizations of alkali electrons and noble-gas nuclei for the case of full polarization. When operating in the SC regime, a bias field of  $B_z^c = -\tilde{B}_z^e - \tilde{B}_z^n$  is applied [4].

To realize an ultrahigh sensitivity of the SC comagnetometer, it is essential to characterize the transverse magnetic field suppression in the SC regime. We define a suppression factor  $SF_x$  ( $SF_y$ ) as the ratio of the scale factors for the response to magnetic field  $B_x$  ( $B_y$ ) and the response to a pseudomagnetic signal (e.g., inertial rotation  $\Omega_y$ ) [30].  $SF_x$  is about 1 order of magnitude worse than  $SF_y$  [31]. Improving the  $SF_x$  is more important for the overall performance, hence we focus on  $SF_x$ :

$$SF_x = \frac{R_2^n + \omega/2 + \omega^2 \hat{\omega}_0^e / (R_2^n \hat{\omega}_0^n)}{\sqrt{(\hat{\omega}_0^n)^2 + (\hat{\omega}_0^e)^2 \omega^2 / R_2^e}}, \quad (2)$$

where  $\omega$  is the angular frequency of the external magnetic field.  $R_2^n$  and  $R_2^e$  are the transverse relaxation rates of noble-gas nuclear spins and alkali electron spins, respectively.  $\hat{\omega}_0^e = \gamma_e \tilde{B}_z^e$  is the electron-spin Larmor precession frequency under  $\tilde{B}_z^n + B_z^c = \tilde{B}_z^e$ , while  $\hat{\omega}_0^n = \gamma_n \tilde{B}_z^n$  is the nuclear spin under  $\tilde{B}_z^e + B_z^c = \tilde{B}_z^n$ . The precession frequencies of coupled electron and noble-gas nuclear spins are combinations of  $\hat{\omega}_0^e$  and  $\hat{\omega}_0^n$  [20]. From Eq. (2), there are three subregimes by considering the critical parameters  $R_2^n$  and  $\omega$ :

$$SF_x \approx \omega / \hat{\omega}_0^n, \quad R_2^n \ll \hat{\omega}_0^n \quad (3)$$

$$SF_x \approx R_2^n / \hat{\omega}_0^n, \quad R_2^n \lesssim \hat{\omega}_0^n, \quad \omega < R_2^n, \quad (4a)$$

$$SF_x \approx (R_2^n + \omega) / \hat{\omega}_0^n, \quad R_2^n \lesssim \hat{\omega}_0^n, \quad \omega > R_2^n. \quad (4b)$$

Previous work [4,32] described the SC regime in case (3) because  $R_2^n$  was considered to be small for K- $^3\text{He}$ . Intriguingly, for the Rb- $^{21}\text{Ne}$  and Cs(Rb)- $^{129}\text{Xe}$  system, case (4) is found primarily relevant, exhibiting a significant difference to K- $^3\text{He}$  systems.

We discuss case (4) as two subcases. In case (4a), the suppression factors  $SF_x$  is limited by the term  $R_2^n / \hat{\omega}_0^n$ . This can be understood from that magnetic noise  $B_\perp$  is compensated by the transverse component of noble-gas nuclear

magnetization  $\tilde{B}_\perp^n$  whose amplitude is determined by  $R_2^n/\hat{\omega}_0^n$ . Case (4a) is  $\omega$  independent, which is contrary to case (3). In case (4b), the  $SF_x$  is limited by  $(R_2^n + \omega)/\hat{\omega}_0^n$ , which can be interpreted as the higher the frequency magnetic noise  $\omega$  is, the harder  $\tilde{B}_\perp^n$  to follow and compensate the  $B_\perp$ , especially for  $\omega$  higher than the intrinsic resonance frequency of noble-gas atoms  $\hat{\omega}_0^n$ . The ways to improve the suppression ability for both subcases is to increase  $\hat{\omega}_0^n$ , i.e.,  $P_z^n$ , and reduce  $R_2^n$ . In the following, we define two parameters  $SF_x^{\text{low}}$  and  $SF_x^{\text{mid}}$ , which are the values of  $SF_x$  in cases (4a) and (4b), respectively.

The SC model has been applied to  $^{21}\text{Ne}$ -Rb-K comagnetometer. In the bottom coordinate of Fig. 1(b), the nuclear spin polarization  $P_z^n$  is improved by increasing the pump light intensity.  $SF_x^{\text{low}}$  and  $SF_x^{\text{mid}}$  decrease with  $P_z^n$ , in agreement with the dependence of  $SF_x$  on  $\hat{\omega}_0^n \propto P_z^n$ . In the top coordinate of Fig. 1(b) when increasing the cell temperature, the  $P_z^n$  and the  $R_2^n$  all increase. The  $R_2^n$  affects the  $SF_x$  in the low-frequency range more significantly than the  $P_z^n$ , leading to that  $SF_x^{\text{low}}$  deteriorates with  $R_2^n$  regardless of the corresponding increment of  $P_z^n$ .

To explain the observed values of  $R_2^n$ , we estimated the partial rates from several known relaxation mechanisms [24,33], including spin-exchange and spin-destruction collisions and magnetic field gradients, and found that their sum of about  $1 \times 10^{-3} \text{ s}^{-1}$  is significantly smaller than the measured value. We find that the observed relaxation rate is, in fact, dominated by the Fermi-contact-interaction field gradient  $\nabla \tilde{B}_z^e$  coming from the polarization gradient  $\nabla P_z^e$  of alkali spins in the SC regime, see Eq. (1). The value of  $\nabla \tilde{B}_z^e$  is calculated to be tens of nT/cm, much higher than the real magnetic field gradient of  $\nabla B_z \approx 2 \text{ nT/cm}$ . Adding this contribution to the gradient-related relaxation [34] brings the calculated value of  $R_2^n$  to agreement with the measurement. Since  $\nabla \tilde{B}_z^e$  has a high-order nonuniform in HSEOP, it cannot be effectively compensated by a uniform gradient coil.

In HSEOP, the polarization gradient  $\nabla P_z^e$  is mainly determined by the ratio of alkali number densities  $\xi = n_{\text{Rb}}/n_{\text{K}}$ . We characterize the relationship between the polarization distribution of electron and nuclear spins and the  $\xi$ . The diffusion of alkali and noble-gas atoms, the inhomogeneity and attenuation of pump light, cell geometry, and wall relaxation are considered to simulate the spin-polarization distribution using finite-element analysis [35,36].

In the simulation,  $P_z^e$  at the cell center is normalized to 0.5 to optimize the sensitivity. The pump light beam has a Gaussian profile with an 18 mm beam diameter to cover the 12 mm diameter spherical cell. The cell is filled with 2280 torr  $^{21}\text{Ne}$  and 50 torr  $\text{N}_2$ . Other parameters of the  $^{21}\text{Ne}$ -Rb-K spin ensembles are the same as in Refs. [28,33]. As shown in Fig. 2(a), for a small  $\xi$ ,  $P_z^e$  decreases significantly along  $\hat{z}$  (the pumping direction), while for a larger  $\xi$ ,  $P_z^e$  becomes more uniform. In comparison,  $P_z^n$  is

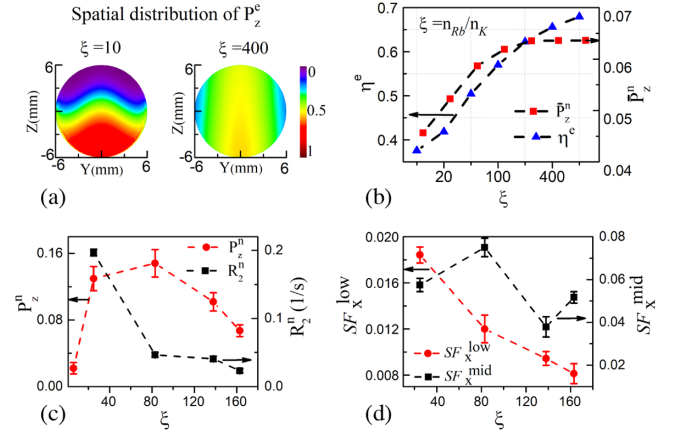


FIG. 2. (a) The simulated spatial distribution of electron polarization  $P_z^e$  for density ratio  $\xi$  of 10 and 400, respectively, in the Y-Z plane of the cell center at 190 °C. (b) The calculated homogeneity factor  $\eta^e$  of  $P_z^e$  and the volume-averaged nuclear polarization  $\bar{P}_z^n$  as functions of  $\xi$ .  $\eta^e \approx 1$  and  $\bar{P}_z^n \approx 0.5$  are not plotted here. (c) The noble-gas spin polarization  $P_z^n$  and transverse relaxation rate  $R_2^n$  as a function of  $\xi$  at 200 °C. By optimizing the  $\xi$ , the  $P_z^n$  and the  $T_2^n = 1/R_2^n$  are improved by nearly 1 order of magnitude, respectively. (d) The averaged suppression factors  $SF_x^{\text{low}}$  and  $SF_x^{\text{mid}}$  as a function of the  $\xi$  at 200 °C.

always spatially homogeneous, because the diffusion rate of noble gas is faster than its relaxation rate. We use  $\eta^e = \bar{P}_z^e/P_{z,\text{Max}}^e$ , the ratio of the volume-averaged value to the maximum value to characterize the homogeneity of the polarization. Figure 2(b) shows the dependence of  $\eta^e$  and the volume-averaged nuclear spin polarization  $\bar{P}_z^n$  on the  $\xi$ . The  $\bar{P}_z^n$  saturates at  $\xi \approx 100$  while  $\eta^e$  continues to increase.

Five  $^{21}\text{Ne}$ -Rb-K cells with different  $\xi = 6, 25, 83, 138,$  and  $163$  were tested, respectively. Apart from  $\xi$ , other parameters were kept nearly the same, i.e.,  $^{21}\text{Ne}$  density about  $2.67 \sim 3.24 \text{ amg}$  and  $\text{N}_2$  pressure about  $35\text{--}53 \text{ torr}$ . As shown in Fig. 2(c),  $P_z^n$  for each cell increases with  $\xi$  but reaches the maximum at approximately  $\xi = 83$  and then decreases, which is different from the simulation result in Fig. 2(b). The difference is due to the fact that  $P_z^e$  in the simulations of  $\bar{P}_z^n$  is set to 0.5 for different  $\xi$ , while in the experiment, the available pump-light intensity is insufficient for the cell with larger  $\xi$  to achieve high  $P_z^e$ , yielding to a smaller  $P_z^n$ . With the increase of the pump-light intensity,  $P_z^n$  can increase for larger  $\xi$ . Because  $P_z^n$  is small for the cell with  $\xi = 6$ , we focus on the cells with  $\xi$  ranging from 25 to 163. Figure 2(c) shows the relationship between  $R_2^n$  and  $\xi$  for a range of pump light intensities.  $R_2^n$  decreases with  $\xi$  due to the reduction of FCI gradient with  $\xi$ , which agrees with the theoretical expectation in Fig. 2(b).

The suppression factors  $SF_x$  for these four cells are shown in Fig. 2(d).  $SF_x^{\text{low}}$  is mostly dominated by  $R_2^n$ , while the behavior of  $SF_x^{\text{mid}}$  appears to be more complicated as it depends on  $R_2^n$ ,  $\omega$  and  $P_z^n$ . Although  $\xi = 83$  achieves the

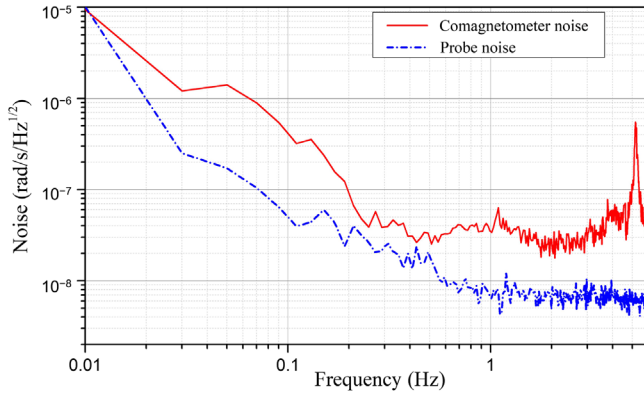


FIG. 3. The noise spectrum of the SC comagnetometer. In the frequency range from 0.2 to 1.0 Hz, the averaged noise is  $3 \times 10^{-8}$  rad/s/Hz $^{1/2}$ . Below 0.2 Hz, the noise spectrum is dominated by the  $1/f$  noise. The peak in the noise spectrum is due to the vibration, which is confirmed with a precision seismometer. The probe noise is measured with unpolarized spin ensembles by blocking the pump laser.

highest  $P_z^n$ , its suppression ability is not optimal. The reduction of the relaxation rate is relatively more important. The optimal suppression ability occurs when  $\xi = 163$ , which is 1 order of magnitude higher than that of  $\xi = 25$ . The optimal  $SF_x$  is smaller than 0.01, which means the femtoTesla-level magnetic noise in the magnetic shield can be suppressed by 2 orders of magnitude.

The amplitude spectral density of comagnetometer signal is shown in Fig. 3. The sensitivity of the SC comagnetometer is calibrated by measuring the rotation of the Earth [30]. Below 0.2 Hz, the comagnetometer noise is dominated by the  $1/f$  noise. The magnetic noise of the inner ferrite shield is calculated to be about  $2.5f^{-1/2}$  fT ( $f$  in the unit of Hz). Except for the frequency range dominated by  $1/f$  noise, the noise from the ferrite shield exceeds the comagnetometer noise in the low-frequency range, indicating that the magnetic noise is effectively suppressed by the SC effect. Above 1.0 Hz, the polarimetry noise of probe light based on optical rotation is lower than  $2 \times 10^{-8}$  rad/Hz $^{1/2}$ , approaching the limit of photon shot noise [37]. The peak around 5.0 Hz is from the mechanical vibration noise.

The averaged noise is  $3 \times 10^{-8}$  rad/s/Hz $^{1/2}$  in the frequency range from 0.2 to 1.0 Hz, corresponding to an effective pseudomagnetic field sensitivity of  $\delta b^n = 1.5$  fT/Hz $^{1/2}$ . For the exotic-field Zeeman-like pseudomagnetic coupling to  $^{21}\text{Ne}$  nuclear spin, the energy is  $E = \mu_{\text{Ne}} \cdot \mathbf{b}^n$ , yielding an energy resolution of  $\delta E_{\text{Ne}} = 3.1 \times 10^{-23}$  eV/Hz $^{1/2}$ . The energy sensitivity of the exotic field coupling to neutron and proton spins are determined by  $\delta E_{n/p} = \delta E_{\text{Ne}}/\eta_{n/p}$ , where  $\eta_n = 0.58$  and  $\eta_p = 0.04$  are the neutron and proton fraction of spin polarization in  $^{21}\text{Ne}$  atoms [38] respectively. Therefore, the energy

sensitivities of our setup are  $\delta E_n = 5.4 \times 10^{-23}$  and  $\delta E_p = 7.8 \times 10^{-22}$  eV/Hz $^{1/2}$ , respectively.

Taking advantage of the ultrahigh sensitivity, this comagnetometer can be used to explore new spin-dependent physics, including directly searching for axion and axion-like particles (ALPs) [10], and local Lorentz invariance (related to the  $CPT$  symmetry) [13,14]. We propose an experiment to search for exotic interaction between the comagnetometer spins and Earth's gravitational field, using the geometry similar to that of Refs. [18,39]. The spin-dependent force could be mediated by an ultralight spin-0 boson (e.g., axion or ALPs) [40–42]:

$$V = \frac{g_s g_p \hbar^2}{8\pi m} (\hat{\sigma} \cdot \hat{r}) \left( \frac{1}{r\lambda} + \frac{1}{r^2} \right) e^{-r/\lambda}, \quad (5)$$

where  $g_s$  and  $g_p$  are scalar and pseudoscalar coupling constants;  $\hbar$  is the reduced Planck constant;  $\hat{\sigma}$  is the Pauli spin-matrix vector of one fermion and  $m$  is its mass;  $\lambda$  is the force range, which is inversely proportional to the mass of the force-mediating boson;  $r$  is the relative distance between two fermions and  $\hat{r}$  is the unit vector directed from the one fermion to the other. If it exists, this exotic force violates parity ( $P$ ) and time-reversal invariance ( $T$ ).

The state-of-art experiments for the proton spin-gravity coupling include the  $^{85}\text{Rb}$ - $^{87}\text{Rb}$  comagnetometer [18] and the  $^{87}\text{Rb}$  hyperfine-level comagnetometer [19]. Both experiments realized energy resolutions on the order of  $10^{-18}$  eV for an integration time of more than one hundred hours. The best experimental result for the neutron-spin coupling to Earth gravity was obtained with a  $^{199}\text{Hg}$ - $^{201}\text{Hg}$  comagnetometer and realized an energy resolution on the order of  $10^{-21}$  eV [39]. We estimate the sensitivity of our experiment using Earth as a source and integrating for about 100 h using a similar approach to the work of Refs. [14,18,39]. The estimated exotic magnetic field sensitivity is  $\delta B \lesssim 0.01$  fT, and energy sensitivity as  $\delta E_n \lesssim 4 \times 10^{-25}$  and  $\delta E_p \lesssim 5 \times 10^{-24}$  eV, respectively. The estimated sensitivity to the coupling constants and comparison with the previous work is shown in Fig. 4. The sensitivity of this proposal can surpass the direct experimental limits and the astrophysical limits on the exotic interactions coupling to proton and neutron spins by more than 4 orders of magnitude.

We established an analytical model to describe the SC effect. The relaxation of noble-gas nuclear spins is found to be dominated by the Fermi-contact-interaction field gradient. The degree of spin polarization and its relaxation time for the noble-gas atoms are both improved by 1 order of magnitude over the earlier work [44] by optimizing the density ratio between the two alkali species. An average sensitivity of  $3 \times 10^{-8}$  rad/s/Hz $^{1/2}$  in the frequency range from 0.2 to 1.0 Hz has been achieved. This sensitivity represents 6 orders of magnitude better energy resolution

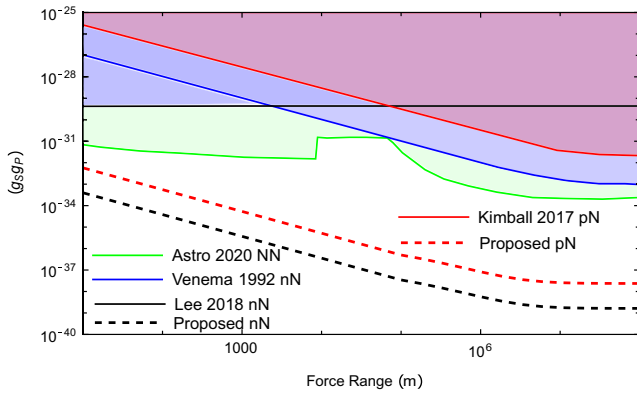


FIG. 4. Existing limits and projected sensitivity on the coupling-constant product  $g_S g_P$  of the spin-dependent force between the neutron (proton) spin and unpolarized nucleon. The black dashed and red dashed lines are the sensitivity in this proposal using the  $^{21}\text{Ne}$  neutron spin and proton spin, respectively. The blue solid line “Venema 1992 nN” [39] and black solid line “Lee 2018 nN” [7] represent the direct experimental limits on the coupling to neutron spins, while the red solid line “Kimball 2017 pN” [18] represents the direct experimental limits on the coupling to proton spins. The green solid line “Astro 2020 NN” [43] represents the astrophysical limits on the coupling between nucleons (not distinguishing between protons and neutrons).

compared to comagnetometers using Rb isotopes that were used to search for exotic gravity coupling to proton spins [18]. The improvement of nuclear spin coherence time and polarization is also beneficial for NMR gyroscopes, noble-gas-spins-based quantum memory, coherent bidirectional coupling between light and noble-gas spins [6], as well as for neutron spin filters [45].

This work is supported by the National Natural Science Foundation of China (NSFC) (Grants No. 62203030 and 61925301 for Distinguished Young Scholars), the China Postdoctoral Science Foundation (Grant No. 2021M700345), the DFG Project ID 390831469: EXC 2118 (PRISMA+ Cluster of Excellence), by the German Federal Ministry of Education and Research (BMBF) within the Quantumtechnologien program (Grant No. 13N15064), and by the QuantERA project LEMAQUME (DFG Project No. 500314265).

\*yanhui.hu@kcl.ac.uk

†wei.ji.physics@gmail.com

[1] W. Terrano and M. Romalis, *Quantum Sci. Technol.* **7**, 014001 (2021).  
 [2] L. Pezze, A. Smerzi, M. K. Oberthaler, R. Schmied, and P. Treutlein, *Rev. Mod. Phys.* **90**, 035005 (2018).  
 [3] D. Budker and M. Romalis, *Nat. Phys.* **3**, 227 (2007).  
 [4] T. W. Kornack, R. K. Ghosh, and M. V. Romalis, *Phys. Rev. Lett.* **95**, 230801 (2005).  
 [5] O. Katz, R. Shaham, and O. Firstenberg, *PRX Quantum* **3**, 010305 (2022).

[6] R. Shaham, O. Katz, and O. Firstenberg, *Nat. Phys.* **18**, 506 (2022).  
 [7] J. Lee, A. Almasi, and M. Romalis, *Phys. Rev. Lett.* **120**, 161801 (2018).  
 [8] W. Ji, Y. Chen, C. Fu, M. Ding, J. Fang, Z. Xiao, K. Wei, and H. Yan, *Phys. Rev. Lett.* **121**, 261803 (2018).  
 [9] M. Bulatowicz, R. Griffith, M. Larsen, J. Mirijanian, C. B. Fu, E. Smith, W. M. Snow, H. Yan, and T. G. Walker, *Phys. Rev. Lett.* **111**, 102001 (2013).  
 [10] S. Afach, B. C. Buchler, D. Budker, C. Dailey, A. Derevianko, V. Dumont, N. L. Figueroa, I. Gerhardt, Z. D. Grujić, H. Guo *et al.*, *Nat. Phys.* **17**, 1396 (2021).  
 [11] M. A. Rosenberry and T. E. Chupp, *Phys. Rev. Lett.* **86**, 22 (2001).  
 [12] N. Sachdeva *et al.*, *Phys. Rev. Lett.* **123**, 143003 (2019).  
 [13] J. M. Brown, S. J. Smullin, T. W. Kornack, and M. V. Romalis, *Phys. Rev. Lett.* **105**, 151604 (2010).  
 [14] M. Smiciklas, J. M. Brown, L. W. Cheuk, S. J. Smullin, and M. V. Romalis, *Phys. Rev. Lett.* **107**, 171604 (2011).  
 [15] D. Sheng, A. Kabcenell, and M. V. Romalis, *Phys. Rev. Lett.* **113**, 163002 (2014).  
 [16] T. Wu, J. W. Blanchard, D. F. J. Kimball, M. Jiang, and D. Budker, *Phys. Rev. Lett.* **121**, 023202 (2018).  
 [17] E. A. Donley, *IEEE Sensors J.* **17** (2010).10.1109/ICSENS.2010.5690983  
 [18] D. F. J. Kimball, J. Dudley, Y. Li, D. Patel, and J. Valdez, *Phys. Rev. D* **96**, 075004 (2017).  
 [19] Z. Wang, X. Peng, R. Zhang, H. Luo, J. Li, Z. Xiong, S. Wang, and H. Guo, *Phys. Rev. Lett.* **124**, 193002 (2020).  
 [20] T. W. Kornack and M. V. Romalis, *Phys. Rev. Lett.* **89**, 253002 (2002).  
 [21] I. Komins, T. Kornack, J. Allred, and M. V. Romalis, *Nature (London)* **422**, 596 (2003).  
 [22] G. Vasilakis, J. M. Brown, T. W. Kornack, and M. V. Romalis, *Phys. Rev. Lett.* **103**, 261801 (2009).  
 [23] E. Klinger, T. Liu, M. Engler, A. Wickenbrock, M. Padniuk, S. Pustelny, T. Kornack, D. F. J. Kimball, and D. Budker, *arXiv:2210.07687*.  
 [24] R. K. Ghosh and M. V. Romalis, *Phys. Rev. A* **81**, 043415 (2010).  
 [25] K. Wei, T. Zhao, X. Fang, Z. Xu, Y. Zhai, W. Quan, and B. Han, *Opt. Express* **28**, 32601 (2020).  
 [26] S. J. Seltzer, Ph.D. dissertation, Princeton University, 2008.  
 [27] E. Babcock, I. Nelson, S. Kadlecck, B. Driehuys, L. W. Anderson, F. W. Hersman, and T. G. Walker, *Phys. Rev. Lett.* **91**, 123003 (2003).  
 [28] J. Lee, Ph.D. dissertation, Princeton University, 2019.  
 [29] K. Wei, T. Zhao, X. Fang, H. Li, Y. Zhai, B. Han, and W. Quan, *Phys. Rev. Appl.* **13**, 044027 (2020).  
 [30] K. Wei, W. Ji, C. Fu, A. Wickenbrock, V. V. Flambaum, J. Fang, and D. Budker, *Nat. Commun.* **13**, 7387 (2022).  
 [31] See Supplemental Material at <http://link.aps.org/supplemental/10.1103/PhysRevLett.130.063201> for details of the working principle of comagnetometers in the SC regime, the experimental apparatus, and suppression factor measurement.  
 [32] J. M. Brown, Ph.D. dissertation, Princeton University, 2011.  
 [33] R. K. Ghosh, Ph.D. dissertation, Princeton University, 2009.  
 [34] G. D. Cates, S. R. Schaefer, and W. Happer, *Phys. Rev. A* **37**, 2877 (1988).

- [35] Y. Jia, Z. Liu, B. Zhou, X. Liang, W. Wu, J. Peng, M. Ding, Y. Zhai, and J. Fang, *J. Phys. D* **52**, 355001 (2019).
- [36] A. Fink, D. Baumer, and E. Brunner, *Phys. Rev. A* **72**, 053411 (2005).
- [37] M. P. Ledbetter, I. M. Savukov, V. M. Acosta, D. Budker, and M. V. Romalis, *Phys. Rev. A* **77**, 033408 (2008).
- [38] A. Almasi, J. Lee, H. Winarto, M. Smiciklas, and M. V. Romalis, *Phys. Rev. Lett.* **125**, 201802 (2020).
- [39] B. J. Venema, P. K. Majumder, S. K. Lamoreaux, B. R. Heckel, and E. N. Fortson, *Phys. Rev. Lett.* **68**, 135 (1992).
- [40] J. E. Moody and F. Wilczek, *Phys. Rev. D* **30**, 130 (1984).
- [41] B. A. Dobrescu and I. Mocioiu, *J. High Energy Phys.* **11** (2006) 005.
- [42] P. Fadeev, Y. V. Stadnik, F. Ficek, M. G. Kozlov, V. V. Flambaum, and D. Budker, *Phys. Rev. A* **99**, 022113 (2019).
- [43] C. A. O'Hare and E. Vitagliano, *Phys. Rev. D* **102**, 115026 (2020).
- [44] H. Pang, W. Fan, J. Huang, F. Liu, S. Liu, and W. Quan, *IEEE Trans. Instrum. Meas.* **71**, 1 (2022).
- [45] J. Zhang, C. Huang, Z. Qin, F. Ye, S. M. Amir, A. Salman, Y. Dong, L. Tian, Z. N. Buck, W. Kreuzpaintner *et al.*, *Sci. China Phys.* **65**, 1 (2022).